Particle Filter Based Prognostics of PEM Fuel Cell Under Constant Load

MayankShekhar JHA*‡, MathieuBressel**,BelkacemOuld-Bouamama***

Genevieve Dauphin-Tanguy**,MickaelHilairet****Daniel Hissel****

*Institut Clément Ader, 3 rue Caroline Aigle 31400 Toulouse CEDEX 04, France

**CRIStALUMR CNRS 9189, Ecole Centrale de Lille, Cité Scientifique 59650 Villeneuve d'Ascq France

***CRIStAL UMR CNRS 9189, Polytech Lille, Cité Scientifique 59650 Villeneuve d'Ascq, France

****FEMTO-ST, UMR CNRS 6174, FCLAB, FR CNRS 3539, Rue Thierry Mieg, 90000 Belfort, France

(jha.mayank.jha@gmail.com, bressel.mathieu@gmail.com,Belkacem.Ouldbouamama@polytech-lille.fr, genevieve.dauphin-tanguy@ec-lille.fr, mickael.hilairet@univ-fcomte.fr,daniel.hissel@univ-fcomte.fr

‡Corresponding Author; First Author,Institut Clément Ader,
3 rue Caroline Aigle 31400 Toulouse CEDEX 04, France.
Tel : +33660673251, jha.mayank.jha@gmail.com

Received: 29.02.2016-Accepted:21.05.2016

Abstract— This paper develops an efficient solution towards the prognostics of industrial Proton Exchange Membrane Fuel Cell (PEMFC). It involves employment of an efficient multi-energetic model suited for diagnostics and prognostics, developed in Bond Graph (BG) framework. The Electrical-Electrochemical (EE) part constitutes the main focus for the problem of prognostics, wherein deviation of the global resistance and limiting current inspires a statistical linear degradation model (DM), under constant current solicitation conditions. The benefits of Particle Filters (PF) is integrated with the BG model derived Analytical Redundancy Relations (ARRs), for the prognostics of the electrical-electrochemical (EE) part. The prognostic problem is formulated as the joint state-parameter estimation problem in Particle Filter framework. Using PF algorithms,estimation of State of Health (SOH) is obtained along with the estimation of the associated parameter that influences the rate of degradation, in probabilistic terms. A simplified variance adaptation scheme is employed to ameliorate the accuracy of remaining useful life (RUL) predictions. Influence of variance adaptation on SOH estimation as well as RUL prediction is assessed. It is shown that a proportional type of variance control leads to better accuracy in RUL predictions accompanied with precise confidence bounds. As the degradation data is obtained from a real industrial PEMFC, the economic viability of this approach for prognostics of PEMFC is significantly high.

Keywords— Prognostics, Bond Graph, Particle Filters, PEM Fuel Cell, Remaining Useful Life

1. Introduction

The presence of irreversible degradation severely degradesthe useful life of Proton Exchange Membrane Fuel Cell (PEMFC) and leads to inefficiency, lesser power density and high maintenance cost [1]. Numerous factors prevent the

wide utility of PEMFC, few of them being: irreversible degradation mechanisms, dehydration of the membrane, catalytic degradation, ripening of the platinum particles and many more [2]. These phenomena usually result in significant voltage drops that are difficult to forecast when a specific load profile of current is considered [3]. Moreover, most of these phenomena are mutually dependent and involve multiple energetic couplings[4].

Prognostics is the science of predicting the Remaining Useful Life (RUL) of a system [5]. The issue of predicting the RUL is efficiently addressed in the realms of Prognostic and Health Management (PHM)[6]. There are several benefits of the latter. For example, the RUL of a fleet of energy sources (e.g. batteries and PEMFCs) may lead to estimation of the power that can be delivered to adapt the energy distribution. This in turn will drastically increase the service life of the system. Moreover, efficient pro-active maintenance strategies may be constructed based upon such a valuable information[6]. There have been a variety of attempts to assess perform accurate prognostics of PEMFC. Data driven techniques and numerous machine learning techniques have been used for that purpose[7, 8]. The main limitation with the latter is the limited insight into the underlying physics of degradation. This motivates employment of either model based prognostics[6] or hybrid prognostics[5, 9]. Hybrid prognostics integrate the advantages of model based and learning techniques, wherein behavioural models or statistical based Degradation Models (DMs) are used for State of Health (SOH) estimation. The measured information is used to update the SOH.

Recently there have been significant endeavors to tackle the issue of failure prediction in the context of PEMFC, from the perspectives of modelbased or hybrid prognostics. There are mainly two major ways of soliciting the stack: constant current load and dynamic current load. While dynamic load remains more realistic in nature and represents closely the load profiles found in practice, constant load is often employed for analysis of prognostics oriented methodologies. This is done to avoid the complexity brought in by the changing ambient conditions. Under constant current solicitation, the hypothesis can be analyzed suitably, after which it can be tested under dynamic solicitations.[10]proposed the exploitation of Extended Kalman Filters (EKFs) under constant current solicitations. Moreover, EKF was also exploited for prognostication while PEMFC remained under dynamic current solicitations [11]. [12]exploited statistical log-linear DMs and Particle Filters (PF) for estimation of SOH estimationsand RUL predictions.[13] employs DM of the Electro-Chemical Active Surface Area (ECSA) for damage tracking and RULprediction using Unscented Kalman Filters.

In the general context of prognostics, last decade has witnessed a tremendous increase in usage of Particle filters for efficient SOH estimation and accurate RUL predictions with precise confidence bounds[14]. Some of the significant works involving PF include : lithium-ion batteries [15], battery health monitoring [16], crack growth prognostics [17], pneumatic valve prognostics [18], wear prognostics in centrifugal pumps[19] etc. A comprehensive study that details various optimal or sub-optimal filters for prognostic purposes is found in [20-22]. On the other hand, to model the complex systems involving extreme non-linear processes (including thermo-chemical phenomena) Bond Graph (BG) modelling technique has been exploited voraciously used owing to the behavioural, structural and causal properties[23].

The latter provide a systematic approach towards development of supervision and fault detection and Isolation (FDI) of highly non-linear and complex thermo-chemical systems [24-26]. In BG framework, the model based FDI is mainly based upon ARRs [27-29]. For deterministic systems, the properties and ARR generation algorithm are well detailed in [27].[30] and[31] develop a detailed PEMFC BG model. [32] develops Signed BG model of PEMFC, but for diagnostics purposes only. As PEMFC involves complex non-linear phenomena belonging to various energetic domains, it is interesting as well as beneficial to employ a suitable BG model to depict the degradation phenomenon. Various motivations that propel this work are:

- BG models developed for PEMFC can be used in combination with associated supervision techniques (ARR generation method) to depict the parametric degradation.
- PFs being a sequential Monte Carlo technique promises to produce better SOH estimations than the other estimators (like EKF) especially in the presence of non-linear underlying process and noises.
- Recently, [33]has proposed a hybrid prognostic methodology that integrates the benefits of BG modelling and PF algorithms for efficient RUL predictions. Application of the method in PEMFC context may yield very useful results.
- In[33], a simplified variance adaptation scheme has also been proposed and implemented to acquire accurate RUL prediction distributions with precise confidence bounds.

  In this paper, BG model of PEMFC is employed to graphically represent the complex phenomena. The emphasis is laid upon the dynamics and parametric degradation manifesting in the electrical-electrochemical (EE) part. ARR generation technique is used to obtain energetic assessment of this subsystem. Using real degradation data, a linear DM is obtained statistically. The latter represents the deviation in global resistance of PEMFC and limiting current under constant current load profile. Following aspects form the novelties carried by this work: (i) a simplified variance adaptation scheme is applied for amelioration of SOH estimations and RUL predictions; (ii) RUL predictions obtained in presence of variance adaptation are shown to be more accurate.

2. BG Model of PEMFC

The extensively well detailed basic chemistry of PEMFC is not provided in this paper. The latter can be found elaborated in [34]. Instead, a BG model of the global system

is presented in Fig. 1. Therein, effort and flow variables model the power exchange [35]. Moreover, the BG model is developed in preferred derivative causality which promises to be more efficient for FDI purposes as unknown initial condition problem for ARR generation is alleviated[27].

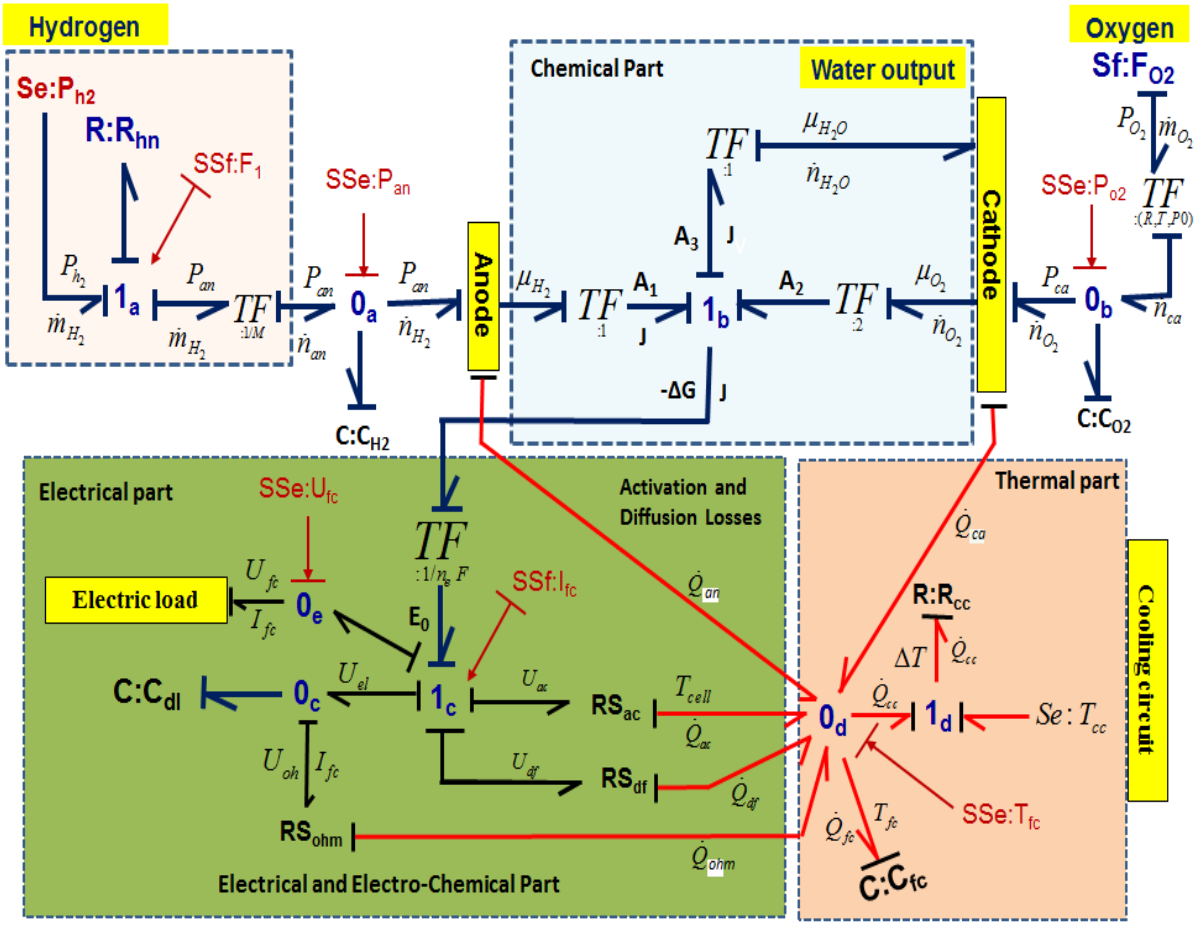

Fig. 1. Bond graph model of the PEMFC inpreferred derivative causality

Additionally, all detectors (*De* for the effort detector and *Df* for the flow detector) are *dualized* into sources of signal *SSe*and *SSf*respectively. The latter are used as inlet nodes in the unknown variable elimination oriented graph [28]. The global system is decomposed into various subsystems: hydrogen inlet, chemical part, oxygen inlet, electrical and electro-chemical part (EE) and thermal part. It should be noted that in this paper, focus remains on EE subsystem only. Assuch, details of modeling aspects and ARR generation process are provided for EE subsystem only. Modeling details of the global model is not presented here which can be found in[36].

The EE subsystem accounts for electrical part and activation-diffusion losses. The reduction-oxidation kinetics (in chemical part, not detailed here) generates an over-voltage. This is known as activation loss. RS is an active two port dissipative (resistive) element which produces thermal energy. The two port thermal dissipative element $\mathbf{RS}_{ohm}$:R_{ohm}models the Ohmic losses (membrane, electrodes and connectors). Moreover, the global resistivity$R_{ohm}$of the membrane-electrode assembly (modelled as $\mathbf{RS}_{ohm}$ in BG) decreases the operational potential due toOhmic effect. The resistance value of the global resistivity R_{ohm}, depends on the degree of humidification of the membrane andtemperature. Asthe chemical reactions progress, consumption of the reactive species leads to loss of partial pressure on the reaction surfaces. Thissignificantly reduces the Nernst potential at high currents. This phenomenon is called diffusionloss. Moreover, during transients, electron accumulation along the membrane electrode interface is observable using Electro Impedance Spectroscopy. Electron accumulation phenomenon typically has the time constant in the orders of micro-seconds. It is termed as double layer capacitance effect. In the BG model, the EE subsystem and the chemical part are connected using the transformer. This results in obtaining the thermodynamic potential as,

$$E_0 = -\frac{\Delta G}{n_e F} = -\frac{A_1 + A_2 - A_3}{n_e F} = \frac{\mu_{H2} + \frac{1}{2}\mu_{O2} + \mu_{H2O}}{n_e F} \quad (0)$$

where$R$ is the perfect gas constant, μ_x is the chemical potential of species x, water is in liquid phase, n_e is the number of electrons involved in the reaction and F is the faraday constant. Moreover,

$$\begin{aligned} \mu_{H2} &= \mu_0^{H2} + RT_{H2}\ln\left(P_{H2}\right) \\ \mu_{O2} &= \mu_0^{O2} + RT_{O2}\ln\left(P_{O2}\right) \\ \mu_{H2O} &= \mu_0^{H2O} \end{aligned} \quad (0)$$

where P_i refers to the partial pressure of specie *i*.The activation and the diffusion phenomenon are modelled, respectively, by the resistor elements:$\boldsymbol{RS}_{\text{ac}}$ and $\boldsymbol{RS}_{\text{df}}$. The power variables are associated as,

$$U_{ac} = RS_{ac}(I_{fc}) = AT\ ln\left(\frac{I_{fc}}{I_0}\right) \quad (0)$$

$$U_{df} = RS_{df}(I_{fc}) = BT\ ln\left(1-\frac{I_{fc}}{I_L}\right) \quad (0)$$

where A is the activation constant $A = R/\chi nF$;B is the diffusion constant: $B = -RT/\chi nF$. Here, χ as the transfer coefficient, I_0 as the exchanged current, I_{fc} as the load current and I_L as the limiting current, i.e., maximal current the fuel cell is able to provide. The double layer capacitance phenomenon is modelled by a capacitor element $\mathrm{C}:C_{dl}$ that imposes the dynamics of the activation phenomena. U_{el} is expressed at the junction $\mathbf{0}_{\mathbf{C}}$, as the solution of the equation:

$$I_{fc} = \frac{U_{el}}{R_{ohm}} + C_{dl}\frac{dU_{el}}{dt} \quad (0)$$

where R_{ohm} is the global resistance (membrane and connectors).

2.1. Derivation of Deterministic ARR in EE part

In general, ARR is a constraint expression being a function of system parameters and known variables. ARRs have been generated from BG models for FDI purposes[27]. The residuals are numerical evaluation of ARRs. Under nominal conditions (no degradation of system parameters or variables), the residual value is theoretically equal to zero. Any deviation in the residual value indicates a certain energetic change at the BG junction from which the respective ARR is derived.

In BG context, ARRs are expressed as,

$$ARR:\ f(SSe, SSf, Se, Sf, MSe, MSf, \boldsymbol{\theta}) \quad (0)$$

where $\boldsymbol{\theta}$ is the vector of system parameters. To address the problem in this paper, the ARR is generated from the $\mathbf{1}_{\mathbf{c}}$ junction which corresponds to the assessment of energy balance in EE subsystem.

$$ARR: n_s\left(E_0 - U_{ac} - U_{df} - U_{el}\right) - U_{fc} = 0 \quad (0)$$

where n_s is number of cells in a stack. From (1)-(4), the unknown variables can be eliminated using causal paths and known electro-chemical relations. Then, ARR is expressed as,

$$ARR = n_s\begin{pmatrix}\mu_0^{H2} + RT_{H2}\ln(P_{H2}) + \frac{1}{2}\left[\mu_0^{O2} + RT_{O2}\ln(P_{O2})\right] \\ -\mu_0^{H2O} - R_{ohm}I_{fc} - ATln\left(\frac{I_{fc}}{I_0}\right) - BTln\left(1-\frac{I_{fc}}{I_L}\right)\end{pmatrix} - SSe:U_{fc}$$

$$= n_s\left(E_0 - R_{ohm}I_{fc} - AT\ln\left(\frac{I_{fc}}{I_0}\right) - BT\ln\left(1-\frac{I_{fc}}{I_L}\right)\right) - SSe:U_{fc}$$

As remarked earlier, it should be noted that while the electrical dynamics remain in the orders of micro-seconds, the degradation phenomena exhibits the time constants in orders of hours. Thus, due to fast electrical dynamics,(5) has been approximated as[37]:

$$U_{el} = R_{ohm}.I_{fc}$$

3. Degradation Model

In this work, the degradation tests described in [10] are used to obtain the DM. A DM is necessary to enhance the knowledge about degradation trend. Periodically, polarization curve which is the expression of voltage as a function of the current is used to measure the static response of the fuel cell throughout its useful life. The polarization curve is understood as,

$$U_{fc} = n_s\left(E_0 - R_{ohm}I_{fc} - AT\ln\left(\frac{I_{fc}}{I_0}\right) - BT\ln\left(1-\frac{I_{fc}}{I_L}\right)\right) \quad (0)$$

The BG derived ARR of (8) represents such a polarisation curve. Details about degradation tests can be found well detailed in [10]. Also, the test bench described in latter has been exploited for this work. The essential details are listed in Table 1.

Table 1. Operating Conditions

Parameters	Details
Number of cells, n_s	5
Surface	100 cm²
Temperature, *T*	60°C
Anode and cathode stoichiometry ratios	1.5-2
Absolute pressure anode/cathode, P_{H2} & P_{O2}	1.5 bar
Relative humidity anode/cathode	50 %
Nominal current, I_{nom}	70 A
Maximal current I_{max}	140 A

The recorded stack voltage U_{fc} (at sampling period of one hour) is depicted in Fig. 2. The non-linear fitting of the measured polarization curves (during aging) is shown in Fig. 3. Fig. 4shows the evolution of the parameter value (in percentage) with respect to its respective initial value. Construction of Fig. 2, 3 and 4 is well explained in [10].

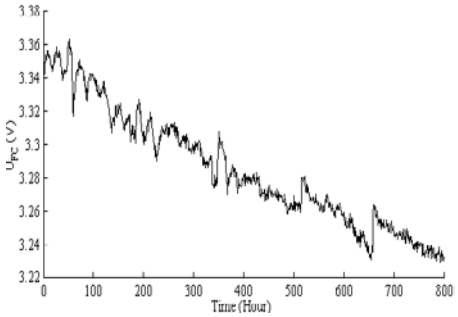

Fig. 2. Recorded voltage

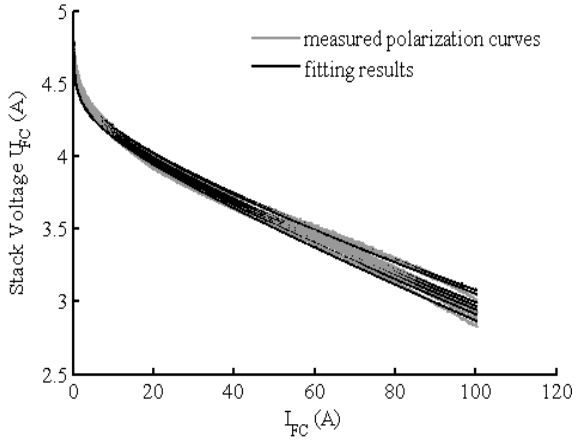

Fig. 3. Polarization Curve and fitting result during ageing

As clearly visible in Fig. 4 , out of the four chosen parameters, significant deviations are reflected in only two parameters: the global resistance R_{ohm} and limit current I_L . In fact, resistance R_{ohm} progresses by more than 12% while the limit current I_L degrades by 13%.

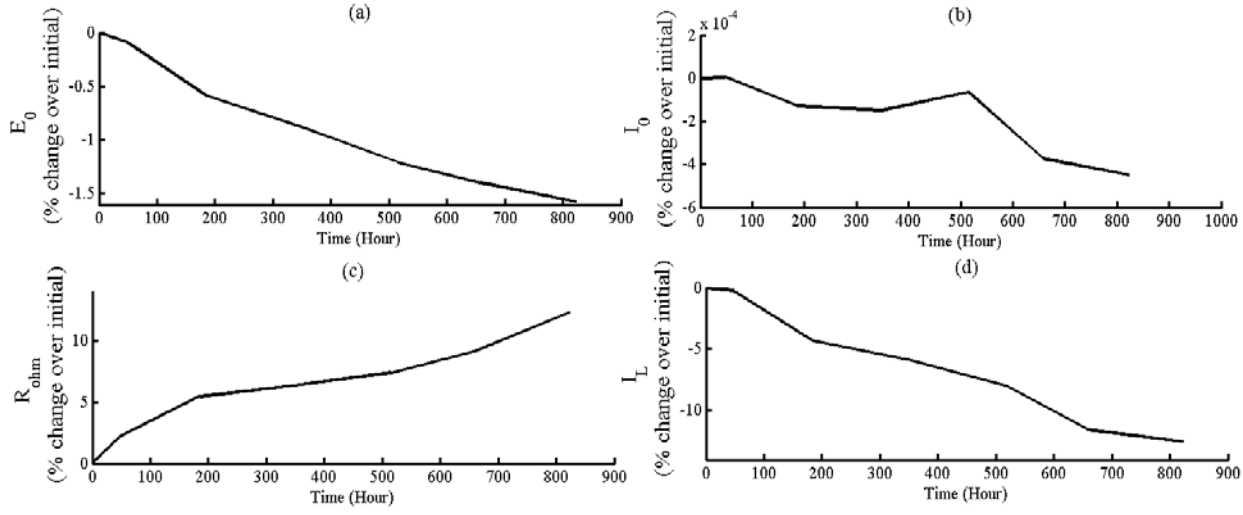

Fig. 4. Deviation of the parameters values (in percentage of their initial value) during aging: (a) Change in E_0 , (b) Change in I_0 , (c) Change in R_{ohm} (d) Change in I_L

As rightly observed in [10], for a given operating condition, only the stack voltage is measured. As such, mutual coupling of global resistance and limiting current is inseparable. The variations in the latter are parameterized with a single parameter α ,a State of Health (SOH) indicator. The variation is expressed in form of linear equation (proposed in [10]) as,

$$R_{ohm}(t) = R_{ohm,n}\left(1+\alpha(t)\right)$$
$$I_L(t) = I_{L,n}\left(1-\alpha(t)\right) \quad (0)$$
$$\alpha(t) = \beta \times t$$

where β explains the approximately constant rate-change of α and sub-script *n* denotes the nominal value.

4. Particle Filter Based Prognostics

The objective of prognostics is achieved by: firstly, evaluating the current state of health; and subsequently, projecting the current state of health in future to assess the RUL. In our context, evaluation of SOH translates to a precise estimation of α and β. This in turn is obtained by formulating the estimation problem in PF framework. In this paper, PF is not described. The method can be found elaborately detailed in [38]. Moreover, the estimation procedure followed here corresponds well with the estimation-RUL prediction routine employed in[33]. Also,*Sampling Importance Resampling* (SIR) PF is employed for estimation.The latter can be found well detailed in [38].

State Equation: In discrete time step $k \in \mathbb{N}$,the fault model can be described in stochastic framework as,

$$\alpha_k = \alpha_{k-1} + \beta_{k-1} \times \Delta t + v_{k-1} \quad (0)$$
$$\beta_k = \beta_{k-1} + \xi_{k-1} \quad (0)$$
$$y_k^d = h\left(\alpha_k, \beta_k\right) + w_k^d$$

where, $v_k \sim \mathrm{N}(0, \sigma_v^2)$ is the associated process noise, $\xi_k \sim \mathrm{N}(0, \sigma_\xi^2)$ israndom walk noise, Δt is the sample time, y_k^d is the measurement obtained from the observation equation(13),$h(\cdot)$is any non-linear function that links the state variables to the observation equationand $w_k^d \sim \mathrm{N}(0, \sigma_{w^d}^2)$ is measurement noise. The fault model is assumed to follow the first order Markov dynamics. The estimation of the current health is obtained by formulating the problem as a joint estimation problem. In particle filter (PF) framework, the estimation at discrete time *k* is obtained as *probability density function* (PDF) $p(\alpha_k, \beta_k \mid y_{k:0}^d)$,based upon history of measurements from initial time, $y_{0:k}^d$. Measurements y_k^d are assumed conditionally independent given the state process. The likelihood function is given as,

$$p(y_{0:k}^d \mid \alpha_k, \beta_k) = \frac{1}{\sigma_{w_k^d}\sqrt{2\pi}} \exp\left(-\left(y_k^d - h\left(\alpha_k, \right.\right.\right. \quad (0)$$

Observation Equation: The measurement of the state health can be obtained implicitly from $ARR: r(t)$. The latter is exploited to obtain the observation equation. Considering R_{ohm} and I_L as the parameters that undergo degradation, ARR can be expressed as,

$$ARR: r(t) = n_s\left(\begin{array}{l} E_0 - \left(R_{ohm,n}\left(1+\alpha(t)\right)\right) I_{fc} - ATln\left(\frac{I_{fc}}{I_0}\right) \\ -BTln\left(1-\frac{I_{fc}}{I_{L,n}\left(1-\alpha(t)\right)}\right) \end{array}\right) - SSe: U_{fc}$$

$$\begin{aligned} r(t) &= n_s\left(E_0 - \left(R_{ohm,n}\right) I_{fc} - ATln\left(\frac{I_{fc}}{I_0}\right) - BTln\left(1-\frac{I_{fc}}{I_{L,n}}\right)\right) - SSe: U_{fc} \\ &\quad + n_s\left(-R_{ohm,n}\alpha(t) I_{fc} - BTln\left(1-\frac{I_{fc}}{I_{L,n}\left(1-\alpha(t)\right)}\right) + BTln\left(1-\frac{I_{fc}}{I_{L,n}}\right)\right) \\ &= r_o(t) + n_s\left(-R_{ohm,n}\alpha(t) I_{fc} - BT\ ln\left(1-\frac{I_{fc}}{I_{L,n}\left(1-\alpha(t)\right)}\right) + BT\ ln\left(1-\frac{I_{fc}}{I_{L,n}}\right)\right) \end{aligned}$$

Here, $r_o(t)$ is the value of ARR while parametric degradation has not started or nominal conditions prevail. This is clear from the fact that in (16) subscript *n* denotes the nominal value of the respective parameter. Power conservation in the ARR leads to,

$$r_o(t) + n_s\left(-R_{ohm,n}\alpha(t) I_{fc} - BT\ ln\left(1-\frac{I_{fc}}{I_{L,n}\left(1-\alpha(t)\right)}\right) + BT\ ln\left(1-\frac{I_{fc}}{I_{L,n}}\right)\right) = 0$$

Thus, measurement of $\alpha(t)$ can be acquired from $r_o(t)$. In discrete time *k*, observation equation is,

$$y^d(k) = r_o(k) = n_s\left(R_{ohm,n}\alpha_k I_{fc} + BT\ ln\left(1-\frac{I_{fc}}{I_{L,n}\left(1-\alpha_k\right)}\right) - BT\ ln\left(1-\frac{I_{fc}}{I_{L,n}}\right)\right) + w_k^d$$

where $w_k^d \sim \mathrm{N}(0, \sigma_{w^d}^2)$ models the noise associated with measurement acquisition. It is approximatedGaussian in nature. σ_{w^d} is approximated from residual measurements during degradation tests.

4.1. State of Health Estimation

The state distribution is approximated by set of discrete weighted samples or particles, $\left\{(\alpha_k, \beta_k), \mathrm{w}_k^i\right\}_{i=1}^N$, where *N* is the total number of particles and the weight associated with each particle is denoted by w_k^i. It should be noted that for i^{th} particle at time *k*, $\left\{(\alpha_k, \beta_k), \mathrm{w}_k^i\right\}$, α_k^i and β_k^i constitute as the estimate of the joint state parameter variables. The posterior density at any time step *k* is approximated as,

$$p(\alpha_k, \beta_k \mid y_{0:k}^d) \approx \sum_{i=1}^{N} \mathrm{w}_k^i . \delta_{(\alpha_k, \beta_k)}(d\alpha_k, d\beta_k)$$

where $\delta_{(\alpha_k, \beta_k)}(d\alpha_k, d\beta_k)$ denotes the Dirac delta function located at (α_k, β_k). Also, $\sum_{i=1}^{N} \mathrm{w}_k^i = 1$. In this paper, the estimation is carried out by employing the *sampling importance resampling* (SIR). It is assumed that $\left\{(\alpha_{k-1}, \beta_{k-1}), \mathrm{w}_{k-1}^i\right\}_{i=1}^N$ are available as realizations of

posterior probability $p(\alpha_{k-1}, \beta_{k-1} \mid y^d_{0:k-1})$ at time $k-1$. The three main steps for estimation procedure are: *prediction*, *state update* and *systematicresampling.* The latter are not detailed here and can be found well explained in [38].

4.1.1. Variance adaptation

As shown in (12), β is modelled as a *random walk process* $\beta_k = \beta_{k-1} + \xi_{k-1}$ where, ξ_{k-1} is sampled from an artificial random zero-mean Gaussian distribution i.e., $\xi_{k-1} \sim \mathrm{N}(0, \sigma^2_{\xi_{k-1}})$.

The artificial random noise is added so that the estimations of β may converge to its respective true value as the estimation process proceeds in time. The noise is generated with a specific variance which essentially determines the magnitude of the diversity of β_{k-1} during the estimation process. While on one hand, variance should be large enough to enable convergence of estimation in sufficiently less amount of time; on the other hand, it should be small enough suchthat tracking of the estimated values is carried out smoothly. Also, magnitude of the variance should allow sufficient amount of diversity in the estimation process. Moreover, in the context of RUL predictions in PF framework, the variance plays an essential role in determining the spread of the RUL predictions. For instance, as shown in[33], a big variance may lead to quick estimation convergence but accompanied with large subsequent spread. The latter eventually leads to large spread in RUL predictions [19]. To ameliorate this aspect, variance adaptation scheme has been proposed, demonstrated and implemented successfully in [19]. Recently, a simplified version of the variance adaptation has been proposed in[33] which builds upon the method of [19] . In this paper, the adaptation scheme described in [33]is followed, wherein it has been described and implemented. The latter is discussed here in brief. Consider the estimated value of β as $\hat{\beta}$ and its true value as β^*. Moreover, consider an interval $\left[\beta^*_l, \beta^*_u\right]$ which contains the true value β^* i.e., $\beta^* \in \left[\beta^*_l, \beta^*_u\right]$. Additionally, the variance of the sampled noise at time *k-1*, $\sigma^2_{\xi_{k-1}}$ is denoted as v^{ξ}_{k-1}, i.e., $\sigma^2_{\xi_{k-1}} \equiv \mathrm{v}^{\xi}_{k-1}$. Associated with the latter, there is a pre-fixed (user dependant) reference variance v^{ξ^*}. The basic philosophy lies in adapting the variance in a proportional control law way.

- Firstly, the variance (spread) is quantified by the statistically robust metric *Relative Median Absolute Deviation* (RMAD) obtained as,

$$RMAD(X) = \frac{\mathrm{Median}_i\left(\left|X_i - \mathrm{Median}_j(\mathrm{X}_j)\right|\right)}{\mathrm{Median}_j(\mathrm{X}_j)} \quad (0$$

where, X_i is an element for any data set *X*.

- The average of mean estimates of $\hat{\beta}$, in a running window of previous *L* estimates is determined as :

$$\bar{\hat{\beta}}_k = \begin{cases} \frac{1}{L+1}\sum_{l=0}^{l=L} \mathrm{mean}(\hat{\beta}_{k-l}) \text{ if } k \geq L \\ \mathrm{mean}(\hat{\beta}_k) \qquad \text{if } k < L \end{cases} \quad (0)$$

The variance adaptation is triggered when the running average $\bar{\hat{\beta}}_k$ is captured inside the interval $\left[\beta^*_l, \beta^*_u\right]$. This insures an automatic adaptation of variance once the estimation mean is around the true value of β.

- Then, the normalised error between the current RMAD v^{ξ}_k (e.g. 80%) and a reference v^{ξ^*} (e.g. 10%) is normalized, and multiplied by a proportional gain constant *P*. Thereafter, the current RMAD v^{ξ}_k is increased or decreased by that amount.
- Finally, the new (adapted) random walk noise ξ_k is obtained by sampling from a zero mean Gaussian distribution with the modified variance v^{ξ}_k obtained in the previous step. It should be noted that choice/magnitude of $\left[\beta^*_l, \beta^*_u\right]$, *P* andinitial variance $\mathrm{v}^{\xi}_{k=0}$ affect the convergence and estimation performance. This aspect has been discussed qualitatively in a detailed manner in[33]. The complete pseudo algorithm (joint estimation and variance adaptation) for SOH estimation is provided in Table II. wherein, $\left\{(\alpha_{k-1}{}^{,i}, \beta_{k-1}{}^{,i}), \mathrm{w}^i_{k-1}\right\}_{i=1}^{N}$ denotes the *i*th particle , w^i_{k-1} denotes the weight of the *i*th particle and N is the number of particles employed in PF.

Table 2. Joint SOH Estimation with Variance Adaptation

Algorithm 1: Estimation using SIR filter and Variance Adaptation Scheme
Inputs: $\left\{(\alpha^i_{k-1}, \beta^i_{k-1}), \mathrm{w}^i_{k-1}\right\}_{i=1}^{N}, y^d_k, \left[\beta^*_l, \beta^*_u\right]$, v^{ξ^*}, *P*, $\mathrm{v}^{\xi}_{k=0}$,
Output: $\left\{(\alpha_k{}^{,i}, \beta_k{}^{,i}), \mathrm{w}^i_k\right\}_{i=1}^{N}$
for *i*=1 to N do
//Variance adaptation
if $k-1 \geq L$
$\bar{\hat{\beta}}_{k-1} \leftarrow \frac{1}{L+1}\sum_{l=0}^{l=L} \mathrm{mean}(\hat{\beta}_{k-1-l})$
else
$\bar{\hat{\beta}}_{k-1} \leftarrow \mathrm{mean}(\hat{\beta}_{k-1})$
end if

if $\overline{\beta}_{k-1} \in \left[\beta_l^*, \beta_u^*\right]$ **then**

$\mathrm{v}_{k-1}^{\xi} = \mathrm{RMAD}\left\{\beta_{k-1}^i\right\}_{i=1}^N$

$\mathrm{v}_{k-1}^{\xi} = \mathrm{v}_{k-1}^{\xi}(1+P\frac{\mathrm{v}_{k-1}^{\xi}-\mathrm{v}^{\xi*}}{\mathrm{v}^{\xi*}})$

else

$\mathrm{v}_{k-1}^{\xi} = \mathrm{v}_{k=0}^{\xi}$

end if

$\xi_{k-1} \leftarrow \mathtt{SampleN}\,(0, \mathrm{v}_{k-1}^{\xi})$

// Estimation

$\alpha_k^{\,i} \sim p(\alpha_k^{\,,i} \mid \alpha_{k-1}^{,i})$

$\beta_k^{\,i} \sim p(\beta_k^{\,,i} \mid \beta_{k-1}^{,i})$

$w_k^i \sim p(y_k^d \mid \alpha_k^{,i}, \beta_k^i)$

end for

$W \leftarrow \sum_{i=1}^{N} w_k^i$

for ***i*****=1 to N do**

$w_k^i \leftarrow w_k^i / W$

end for

$\left\{(\alpha_k^{\,,i}, \beta_k^{\,,i}), \mathrm{w}_k^i\right\}_{i=1}^N \leftarrow \mathrm{RESAMPLE}\left\{(\alpha_k^{\,,i}, \beta_k^{\,,i}), \mathrm{w}_k^i\right\}_{i=1}^N$

4.2. *RUL Prediction*

The RUL prediction is a task accomplished through the knowledge of the time steps required for the current estimate to reach its corresponding failure state. In PF framework, this can be accomplished by projecting each particle in future, until the failure state is obtained. In other words, the particles $\left\{(\alpha_k^{\,,i}, \beta_k^{\,,i}), \mathrm{w}_k^i\right\}_{i=1}^N$ that constitute the joint estimate of $p(\alpha_k, \beta_k)$ are projected (say l steps) ahead in future by simulation of the fault model until $\alpha = \alpha_{fail}$ [12, 18, 19,39]. It should be noted that failure state α_{fail} is pre-fixed and user dependent. The estimation of the state, variance adaptation and RUL prediction step constitute one single iteration step. The RUL prediction algorithm is given in Table III.

Table 3.RUL Prediction

Algorithm 2: RUL Prediction

Inputs: $\left\{(\alpha_k^{\,,i}, \beta_k^{\,,i}), \mathrm{w}_k^i\right\}_{i=1}^N, \alpha_{fail}$

Variable: l

Outputs: $\left\{RUL_k^{\alpha^i}, \mathrm{w}_k^i\right\}_{i=1}^N$

for*i*=1 **to** N **do**

l**=0**

while $\alpha_{k+l}^{,i} \le \alpha_{fail}$ **do**

$\beta_{k+1}^i \sim p(\beta_{k+1}^i \mid \beta_k^i)$

$\alpha_{k+1}^i \sim p(\alpha_{k+1}^i \mid \alpha_k^i, \beta_{k+1}^i)$

$l \leftarrow l+1$

end while

$RUL_k^{\alpha^i} \leftarrow l$

end for

4.3. Evaluation Metrics

In this section, various assessment metrics employed for assessing the prognostics performance are provided. They can be found detailed in [40] and various case studies that discuss the implementation of the same can be found in [19, 39, 41].

Root mean square error (RMSE): This metric is used to express the relative accuracy of the estimation performance:

$$\mathrm{RMSE}_X = \sqrt{Mean_k\left[\left(\frac{mean(X)-X^*}{X^*}\right)^2\right]} \quad (0)$$

where, for species X, X^* denotes the corresponding true values. $Mean_k$ expresses the mean over all values of *k*.

Relative median absolute deviation (RMAD): As shown in (21), RMADdetermines the spread of estimation relative to median as a percentage. It is averaged over multiple values of *k* to obtain,

$$\overline{\mathrm{RMAD}}_\beta = Mean_k(\mathrm{RMAD}_\beta) \quad (0)$$

Here, $Mean_k(\mathrm{RMAD}_\beta)$ is the RMAD of β and $Mean_k$ expresses the mean over all values of *k*. The efficiency of the RUL predictions are demonstrated mostly using the $\alpha-\lambda$ metric[40]. The RUL prediction distributions are assessed against an *accuracy cone* defined by the bounds of the true *RUL* as $(1\pm\alpha)RUL^*$. In fact, $\alpha\in[0,1]$ determines magnitude of uncertainty over the true RUL measure, acknowledged for the assessment. It should be noted that α is an entity different form the SOH indicator $\alpha(t)$. Moreover, $\lambda\in[0,1]$ denotes the fraction of time between the initial prediction time point and the true End of Life. The precision and accuracy of the prognostication is assessed using the *Relative Accuracy* metric [40]. The latter is expressed with respect to a particular prediction time point k_p (time point at which the RUL prediction is generated) as,

$$\mathrm{RA}_{k_p} = \left(1 - \frac{\left| RUL^*_{k_p} - \text{Median } p(RUL_{k_p}) \right|}{RUL^*_{k_p}} \right) \quad (0)$$

The average of the latter over all the prediction time points $\overline{\mathrm{RA}}$ is used to assess the overall accuracy of the RUL prediction process. It is determined as,

$$\overline{\mathrm{RA}} = \text{Mean}_{k_p}\, p(\mathrm{RA}_{k_p}) \quad (0)$$

4.4. Results and Discussion

The degradation model inFig. 4 motivates the failure state α_{fail} to be pre-fixed as $\alpha_{fail} = 0.12$. Choice of the latter is based upon the degradation tests considered in this paper. Such a failure state signifies 12% deviation over the nominal value (initial value). Additionally, according to the linear degradation model of (12), the deviation is assumed to evolve in a perfect linear way. As such, true value of SOH indicator α_{true} evolves linearly such that α_{fail} is reached at end of the degradation test i.e., 900 Hours. Accordingly, true value of slope β_{true} is 1.3×10^{-4}.All the simulations are carried out with N=500 particles in PF. The measurement noise variance $\sigma^2_{w^d}$ is obtained from square of the standard deviation of the $y^d(t)$ measurements recorded during degradation tests, as $\sigma^2_{w^d} = 10^{-6}$.Then, the measurement noise variance in PF is set as 100 times that of residual measurement variance $\sigma^2_{w^d}$. This way a good estimation performance is expected in presence of outliers or un-modelled disturbances [19]. In principle, the value of the process noise σ^2_v can obtained from the DM of (12) (see Fig. 4c) through linear/non-linear regression techniques and associated regression residuals [42]. In order to obtain a smooth estimation, a good value for process noise variance is found through successive tuning as $\sigma^2_v = 10^{-6}$.

The initial random walk noise variance is set as $\mathrm{v}^{\xi}_{k=0} = 10^{-8}$, for a quick convergence. Along with the latter, a good value of $\mathrm{v}^{\xi}_{k=0}$ ensures quick capture of the running average $\overline{\beta}_k$ inside the interval $\left[\beta^*_l, \beta^*_u\right]$[33]. In this work, after a number of simulations it is found that : a running window of *L*=100 previous estimates gives a smooth value of $\overline{\beta}_k$; $\left[\beta^*_l, \beta^*_u\right] = \left[0.5\times10^{-4}, 3\times10^{-4}\right]$ leads to suitable implementation of variance adaptation scheme; a reference RMAD $\mathrm{v}^{\xi*}$ = 20% enables sufficient freedom to estimation variables for appropriate convergence (see the qualitative discussion on efficient tuning of these parameters in[33]).

Proportional gain *P* determines how rapidly the estimation spread is reduced to the reference RMAD $\mathrm{v}^{\xi*}$. To illustrate the influence of *P* on estimation performance, Fig. 5 shows the estimation of β with different values of *P*, with $P = \{0, 1\times10^{-4}, 1\times10^{-3}, 1\times10^{-2}, 1\times10^{-1}\}$. Additionally, the RMAD values for each of the cases are plotted in Fig. 6. Table IV lists the various accuracy gauging details corresponding to various values of *P*. Note that $\overline{\mathrm{RA}}$ metric in Table IV is employed to assess the accuracy of the subsequent RUL predictions obtained for each case. For the sake of comparison, Fig. 8shows the RUL predictions without and with the variance adaptation scheme. Therein, the box plots are employed to describe the prediction distributions. Moreover, the accuracy cone is generated with α=0.4 implying that the amount of RUL probability mass falling within 40% of the true RUL value will be acknowledged to ascertain whether a particular prediction is true or not[40](not considered in this paper).

Following significant observations can be drawn from Fig. 5,Fig. 6 and Table IV :

- Absence of variance adaptation (*P*=0) results in large estimation spread. This large RMAD affects the RUL predictions and the associated accuracy. The RUL predictions obtained without variance adaptation is shown in Fig. 8a. where the prediction distributions have huge spread with considerable outliers. The latter leads to unreliable/imprecise prediction results. This is also reflected in comparatively the lowest value of $\overline{\mathrm{RA}}$ as shown in Table IV.
- With increasing values of *P*, the estimation of RMAD tends to get reduced to the assigned $\mathrm{v}^{\xi*}$.*P*=0.0001 has no considerable effect in reducing the RMAD as shown in Fig. 5b,Fig. 6b and does not improve $\overline{\mathrm{RA}}$ significantly. *P*=0.001 brings down the estimation RMAD (see Fig. 5c); however,the latter is not equal to $\mathrm{v}^{\xi*} = 20\%$ (see Fig. 6c). However, *P*=0.01 has a significant effect in not only bringing down the RMAD to $\mathrm{v}^{\xi*} = 20\%$ (see Fig. 5d), but also sustaining RMAD_{β} at $\mathrm{v}^{\xi*}$ (see Fig. 6d).
- *P*=0.1 is a very large gain value that inhibits the estimation to progress properly by hammering the estimation spread to a very low value (see Fig. 5e and Fig. 6e). The large gain value rapidly cuts the diversity in PF particles and does not lead the estimations to converge to their respective true values. The latter leads to invalid estimation and RUL predictions (see Table IV).

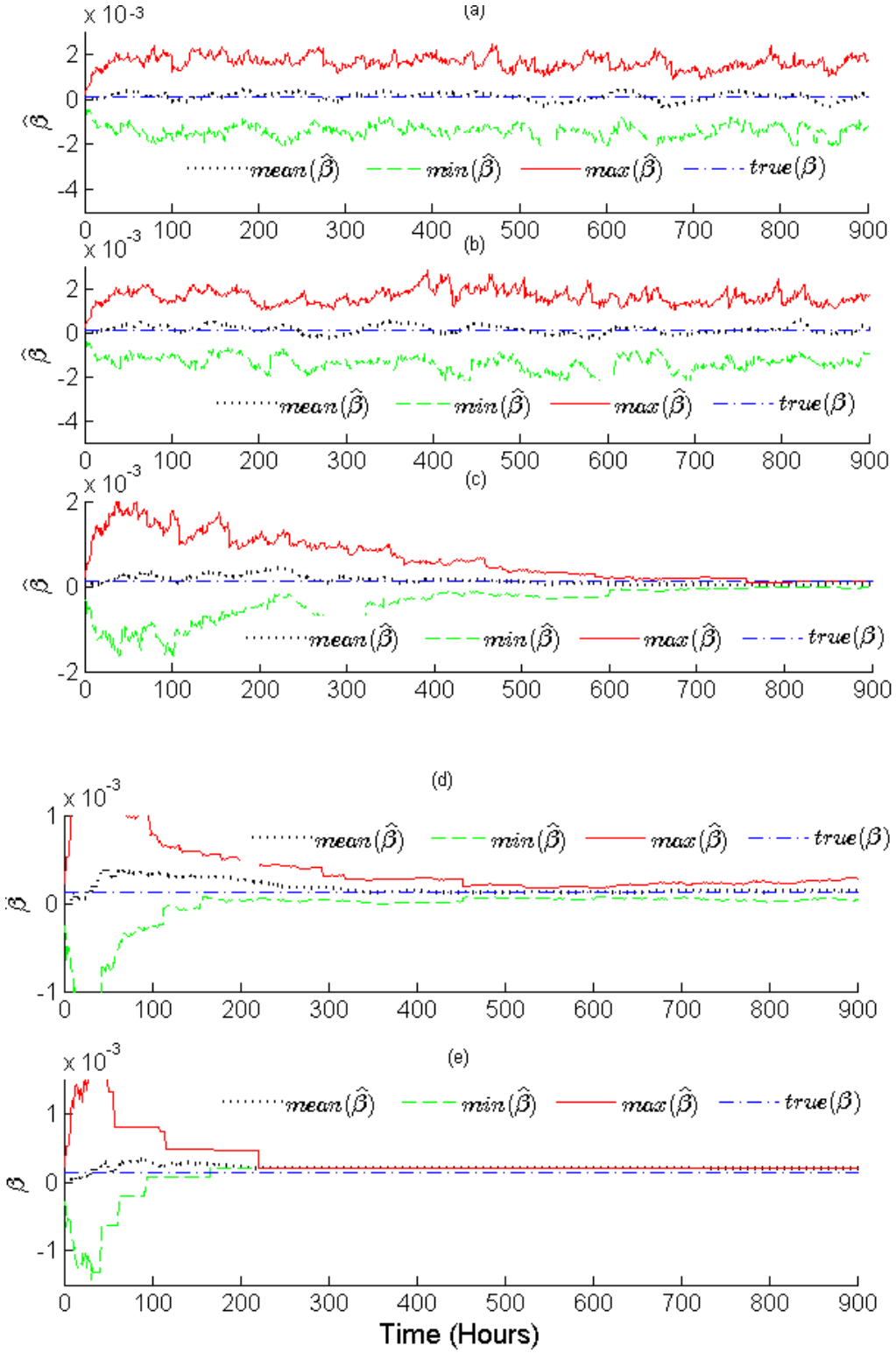

Fig. 5. Influence of Proportional gain *P* of variance adaptation scheme on estimation of β. (a) No variance adaptation *P*=0, (b) *P*=0.0001, (c) *P*=0.001, (d) *P*=0.01, (e) *P*=0.1.

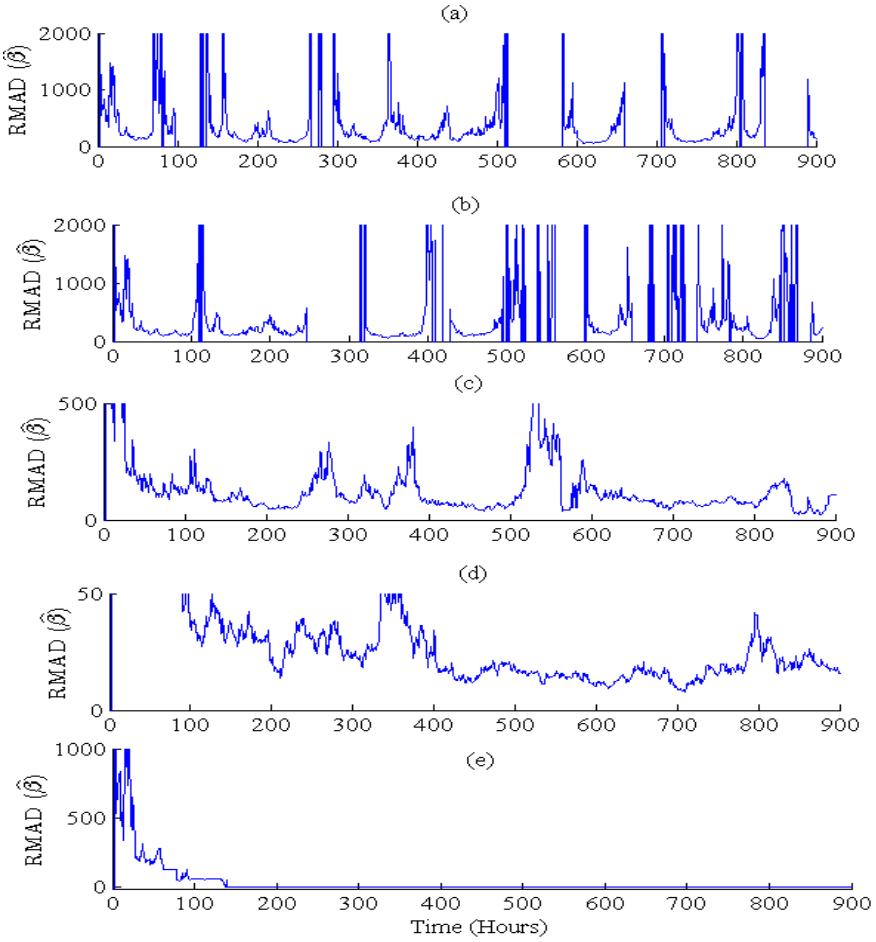

Fig. 6. Influence of different values of Proportional gain *P* considered in Fig. 5 on RMAD values. (a) No variance adaptation *P*=0, (b) *P*=0.0001, (c) *P*=0.001, (d) *P*=0.01, (e) *P*=0.1.

- As clearly visible in Table IV, the variance adaptation scheme does not particularly reduce the estimation accuracy or decrease the RMSE values, but significantly decreases the estimation spread. The latter leads to the desirable increase in prediction accuracy and the number of acceptable RUL predictions.

Table 4. Influence of Different Proportional Gains on Estimation and RUL Prediction

P	$\overline{\text{RMAD}_\beta}$	RMSE_β	$\overline{\text{RA}}$
0	1869.56%	11.65%	36.56%
0.0001	1467.78%	11.04%	43.76%
0.001	95.4.21%	10.28%	67.89%
0.01	17.43%	10.07%	73.43%
0.1	1.32%	Not valid	Not valid

Based on the observations made above, *P*=0.01 is chosen to be an appropriate gain value. Hence, the estimations of SOH α , β and RUL predictions obtained with *P*=0.01 are the prognostic results of this paper. The various estimation errors are listed in Table V. The estimation of SOH and measurements y^d are shown in Fig. 7.

The SOH is estimated with RMSE_α of 24% (see Table V), which does not indicate a good estimation performance. However, it must be remembered that with real experimental data in-use, the true SOH α_{true} is not perfectly linear (see Fig. 4c and d) and β_{true} is not perfectly constant. As such, $RMSE_\alpha$ and $RMSE_\beta$ cannot be regarded as reliable metrics for evaluation of estimation performance. However, $RMSE_{y^d}$ correctly assesses the accuracy of measurement estimation. As clearly shown in Fig. 7b, the residual measurements are estimated with high accuracy and small RMSE. The RUL predictions obtained subsequently are shown in Fig. 8b, wherein the RUL PDFs are presented in box-plot form. As it can be observed, most of the prediction PDFs have less spread owing to the adaptation of the variance. Moreover, most of the prediction PDFs have their medianswithin the accuracy bounds. The latter considerably enhances the accuracy (see Table V).

Table 5. Estimation and RUL Prediction Performance with *P*=0.01

RMSE_α	RMSE_β	RMSE_{y^d}	$\overline{\text{RA}}$
23.57%	8.67%	9.53%	73.43%

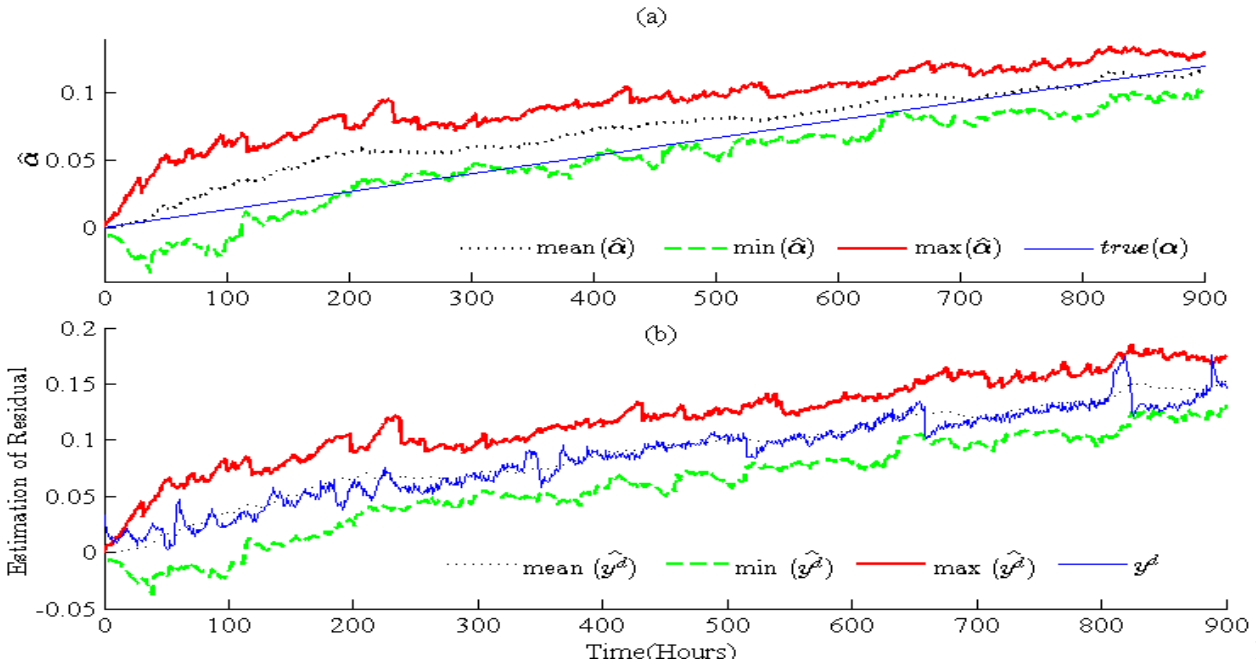

Fig. 7. Estimation of SOH indicator α and residual measurements y^d with the accepted value of proportional gain P=0.01 (a) Estimation of SOH indicator α (b) residual measurements y^d

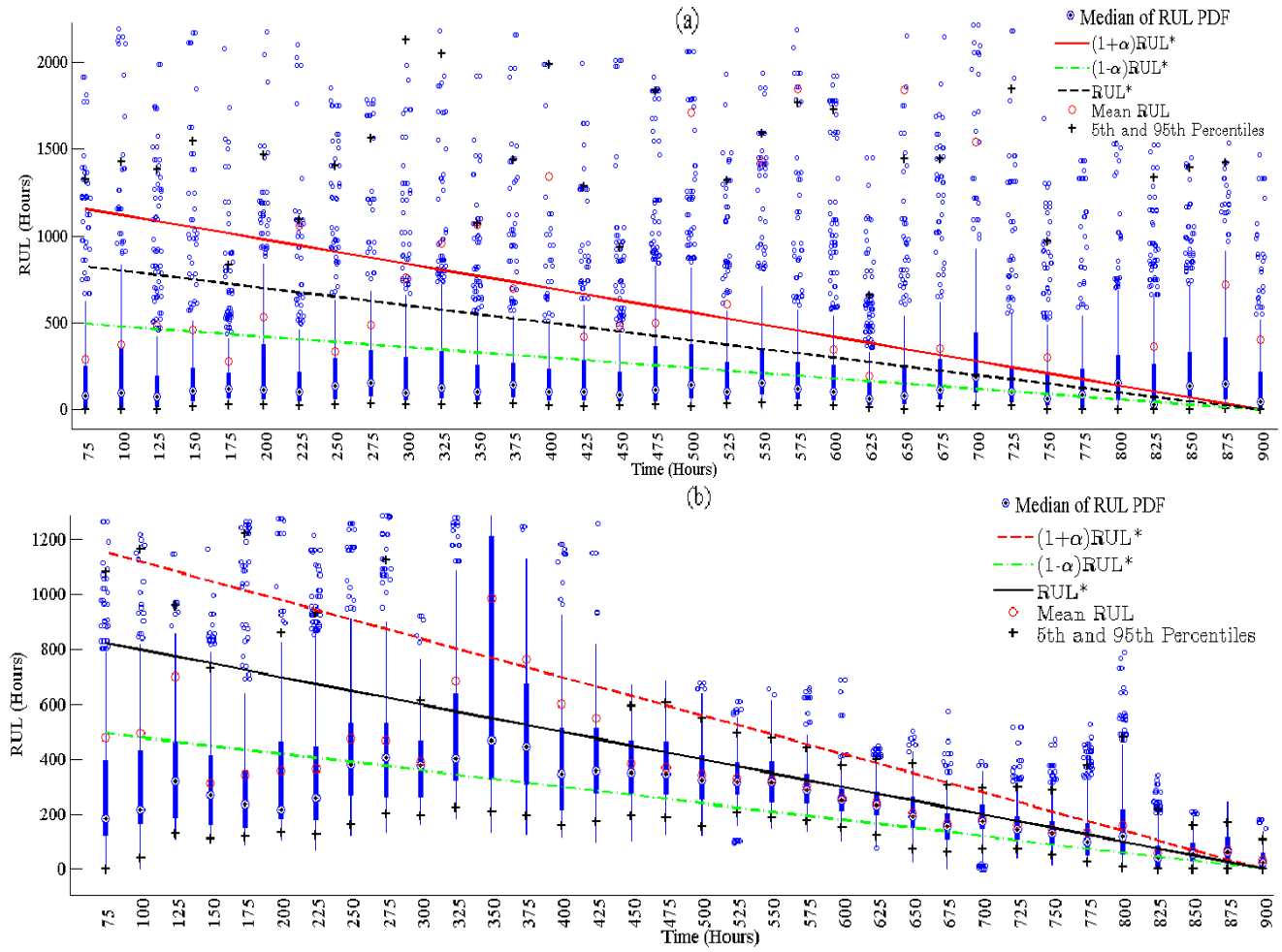

Fig. 8. RUL Predictions (a) Without any variance adaptation P=0, shown here for comparison purposes (b) Accepted RUL prediction with variance adaptation P=0.01 and performance of Table V

5. Conclusions

With real degradation data sets, the methodology applied is able to successfully assess the SOH and predict the RUL with a very high accuracy and precise confidence bounds. Firstly, the BG model is able to depict and model the highly complex inherent phenomena of PEMFC. This leads to efficient and simplified graphical representation. Secondly, ARR sensitive to the EE subsystem provides measurement to the PFs for efficient estimation of SOH and associated hidden parameter that influences the rate of degradation. Thirdly, employment of PF leads to efficient SOH estimation in presence of noisy measurements. The variance adaptation scheme is particularly very useful in increasing the RUL prediction accuracy by reducing the estimation spread. It has been shown that under similar conditions, without variance adaptation, the RUL predictions are sparsely distributed with large spread. As such, they are less accurate and less useful in practice. Although, the prediction accuracy is comparatively high, it can be increased further by amelioration of the estimation accuracy. It should be noted that variance adaptation only affects the estimation spread and does not alleviate the estimation error *per se*. The latter can be achieved by employment of higher number of PF particles. This forms a promising future work. Moreover, number of particles affect the prediction computational time significantly. This aspect has not been analyzed in this paper and forms a very interesting future perspective. Moreover, a comparative study against EKF will be performed in future. Additionally, this method can be extended to integrate the FDI modules already available. This will lead towards a comprehensive health monitoring environment.

Acknowledgment

This work was supported by the project ANR PROPICE (ANR-12-PRGE-0001) and by the project LABEX ACTION (ANR-11-LABX-01-0) both funded by the French National Research Agency.

References

[1] X. Luo, J. Wang, M. Dooner, and J. Clarke, "Overview of current development in electrical energy storage technologies and the application potential in power system operation," Applied Energy, vol. 137, pp. 511-536, 2015.

[2] W. Schmittinger and A. Vahidi, "A review of the main parameters influencing long-term performance and durability of PEM fuel cells," Journal of Power Sources, vol. 180, pp. 1-14, 2008.

[3] P. Pei and H. Chen, "Main factors affecting the lifetime of Proton Exchange Membrane fuel cells in vehicle applications: A review," Applied Energy, vol. 125, pp. 60-75, 2014.

[4] M. Jouin, R. Gouriveau, D. Hissel, M.-C. Péra, and N. Zerhouni, "Degradations analysis and aging modeling for health assessment and prognostics of PEMFC," Reliability Engineering & System Safety, vol. 148, pp. 78-95, 2016.

[5] G. Vachtsevanos, F. Lewis, M. Roemer, A. Hess, and B. Wu, Intelligent Fault Diagnosis and Prognosis for Engineering Systems. New Jersey: John Wiley & Sons, Inc., 2007.

[6] A. K. Jardine, D. Lin, and D. Banjevic, "A review on machinery diagnostics and prognostics implementing condition-based maintenance," Mechanical systems and signal processing, vol. 20, pp. 1483-1510, 2006.

[7] K. Javed, R. Gouriveau, N. Zerhouni, and P. Nectoux, "Enabling health monitoring approach based on vibration data for accurate prognostics," Industrial Electronics, IEEE Transactions on, vol. 62, pp. 647-656, 2015.

[8] K. Javed, R. Gouriveau, N. Zerhouni, and D. Hissel, "Improving accuracy of long-term prognostics of PEMFC stack to estimate remaining useful life," in Industrial Technology (ICIT), 2015 IEEE International Conference on, 2015, pp. 1047-1052.

[9] J. Sikorska, M. Hodkiewicz, and L. Ma, "Prognostic modelling options for remaining useful life estimation by industry," Mechanical Systems and Signal Processing, vol. 25, pp. 1803-1836, 2011.

[10] M. Bressel, M. Hilairet, D. Hissel, and B. Ould Bouamama, "Extended Kalman Filter for prognostic of Proton Exchange Membrane Fuel Cell," Applied Energy, vol. 164, pp. 220-227, 2/15/ 2016.

[11] M. Bressel, M. Hilairet, D. Hissel, and B. Ould Bouamama, "Remaining Useful Life Prediction and Uncertainty Quantification of Proton Exchange Membrane Fuel Cell Under Variable Load," IEEE Transactions on Industrial Electronics, 2016.

[12] M. Jouin, R. Gouriveau, D. Hissel, M.-C. Péra, and N. Zerhouni, "Prognostics of PEM fuel cell in a particle filtering framework," International Journal of Hydrogen Energy, vol. 39, pp. 481-494, 2014.

[13] Y. Wang, K. S. Chen, J. Mishler, S. C. Cho, and X. C. Adroher, "A review of polymer electrolyte membrane fuel cells: technology, applications, and needs on fundamental research," Applied Energy, vol. 88, pp. 981-1007, 2011.

[14] M. E. Orchard, "A particle filtering-based framework for on-line fault diagnosis and failure prognosis," Ph.D dissertation, Georgia Institute of Technology, 2007.

[15] B. Saha and K. Goebel, "Modeling Li-ion battery capacity depletion in a particle filtering framework," in Proceedings of the annual conference of the prognostics and health management society, 2009, pp. 2909-2924.

[16] B. Saha, K. Goebel, S. Poll, and J. Christophersen, "Prognostics methods for battery health monitoring using a Bayesian framework," Instrumentation and Measurement, IEEE Transactions on, vol. 58, pp. 291-296, 2009.

[17] E. Zio and G. Peloni, "Particle filtering prognostic estimation of the remaining useful life of nonlinear

components," Reliability Engineering & System Safety, vol. 96, pp. 403-409, 2011.

[18] M. J. Daigle and K. Goebel, "A Model-Based Prognostics Approach Applied to Pneumatic Valves," International Journal of Prognostics and Health Management, vol. 2, 2011.

[19] M. J. Daigle and K. Goebel, "Model-based prognostics with concurrent damage progression processes," Systems, Man, and Cybernetics: Systems, IEEE Transactions on, vol. 43, pp. 535-546, 2013.

[20] D. An, N. H. Kim, and J.-H. Choi, "Practical options for selecting data-driven or physics-based prognostics algorithms with reviews," Reliability Engineering & System Safety, vol. 133, pp. 223-236, 2015.

[21] M. Daigle, B. Saha, and K. Goebel, "A comparison of filter-based approaches for model-based prognostics," in Aerospace Conference, 2012 IEEE, 2012, pp. 1-10.

[22] B. Saha, K. Goebel, and J. Christophersen, "Comparison of prognostic algorithms for estimating remaining useful life of batteries," Transactions of the Institute of Measurement and Control, 2009.

[23] A. Mukherjee and A. K. Samantaray, Bond graph in modeling, simulation and fault identification: IK International Pvt Ltd, 2006.

[24] K. Medjaher, A. K. Samantaray, B. Ould Bouamama, and M. Staroswiecki, "Supervision of an industrial steam generator. Part II: Online implementation," Control Engineering Practice, vol. 14, pp. 85-96, 1// 2006.

[25] R. Kumar and L. Umanand, "Modeling of a pressure modulated desalination system using bond graph methodology," Applied Energy, vol. 86, pp. 1654-1666, 9// 2009.

[26] M. Tan, L. Chen, J. Jin, F. Sun, and C. Wu, "Bond-graph-based fault-diagnosis for a marine condensate–booster–feedwater system," Applied Energy, vol. 81, pp. 449-458, 8// 2005.

[27] B. O. Bouamama, A. Samantaray, M. Staroswiecki, and G. Dauphin-Tanguy, "Derivation of constraint relations from bond graph models for fault detection and isolation," SIMULATION SERIES, vol. 35, pp. 104-109, 2003.

[28] A. K. Samantaray and B. O. Bouamama, Model-based process supervision: A bond graph approach: Springer Science & Business Media, 2008.

[29] M. Jha, G. Dauphin-Tanguy, and B. Ould Bouamama, "Robust FDI based on LFT BG and relative activity at junction," in Control Conference (ECC), 2014 European, 2014, pp. 938-943.

[30] R. Saisset, G. Fontes, C. Turpin, and S. Astier, "Bond Graph model of a PEM fuel cell," Journal of Power Sources, vol. 156, pp. 100-107, 2006.

[31] C. Peraza, J. G. Diaz, F. J. Arteaga-Bravo, C. Villanueva, and F. Gonzalez-Longatt, "Modeling and simulation of PEM fuel cell with bond graph and 20sim," in American Control Conference, 2008, 2008, pp. 5104-5108.

[32] B. OULDBOUAMAMA, N. CHATTI, and A. GEHIN, "Signed Bond Graph for health monitoring of PEM fuel cell," presented at the 5th International Conference of Development of Fuel Cells, Karlsruhe, Germany, 2013.

[33] M. S. Jha, G. Dauphin-Tanguy, and B. Ould-Bouamama, "Particle filter based hybrid prognostics for health monitoring of uncertain systems in bond graph framework," Mechanical Systems and Signal Processing, vol. 75, pp. 301-329, 6/15/ 2016.

[34] J. Larminie, A. Dicks, and M. S. McDonald, Fuel cell systems explained vol. 2: Wiley New York, 2003.

[35] D. C. Karnopp, D. L. Margolis, and R. C. Rosenberg, System Dynamics: Modeling, Simulation, and Control of Mechatronic Systems: Wiley, 2012.

[36] B. Ould Bouamama, M. Bressel, D. Hissel, and M. Hilairet, "Diagnosability of PEMFC based upon Bond Graph LFT," presented at the 17th International Conference on Electrical and Control Engineering, ICECE, San Francisco, USA, 2015.

[37] F. De Bruijn, V. Dam, and G. Janssen, "Review: durability and degradation issues of PEM fuel cell components," Fuel cells, vol. 8, p. 3, 2008.

[38] M. S. Arulampalam, S. Maskell, N. Gordon, and T. Clapp, "A tutorial on particle filters for online nonlinear/non-Gaussian Bayesian tracking," Signal Processing, IEEE Transactions on, vol. 50, pp. 174-188, 2002.

[39] M. Daigle and K. Goebel, "Model-based prognostics under limited sensing," in Aerospace Conference, 2010 IEEE, 2010, pp. 1-12.

[40] A. Saxena, J. Celaya, B. Saha, S. Saha, and K. Goebel, "Metrics for offline evaluation of prognostic performance," International Journal of Prognostics and Health Management Volume 1 (color), p. 4, 2010.

[41] M. Jha, G. Dauphin-Tanguy, and B. Ould Bouamama, "Integrated Diagnosis and Prognosis of Uncertain Systems: A Bond Graph Approach " in Second European Conference of the PHM Society 2014 -Nantes France, 2014, pp. 391-400.

[42] J. Celaya, C. Kulkarni, G. Biswas, S. Saha, and K. Goebel, "A model-based prognostics methodology for electrolytic capacitors based on electrical overstress accelerated aging," 2011.